RESEARCH ARTICLE | MARCH 18 2025

Dopant vs free carrier concentrations in InAs/GaAs semiconductor quantum dots *⊙*

J. Brubach ^(a); T.-Y. Huang ^(a); T. Borrely ^(a); C. Greenhill ^(a); J. Walrath ^(a); G. Fedele; Y.-C. Yang ^(a); A. Zimmerman ^(b); R. S. Goldman ^(a)



Appl. Phys. Lett. 126, 112107 (2025) https://doi.org/10.1063/5.0244331

A CHORUS





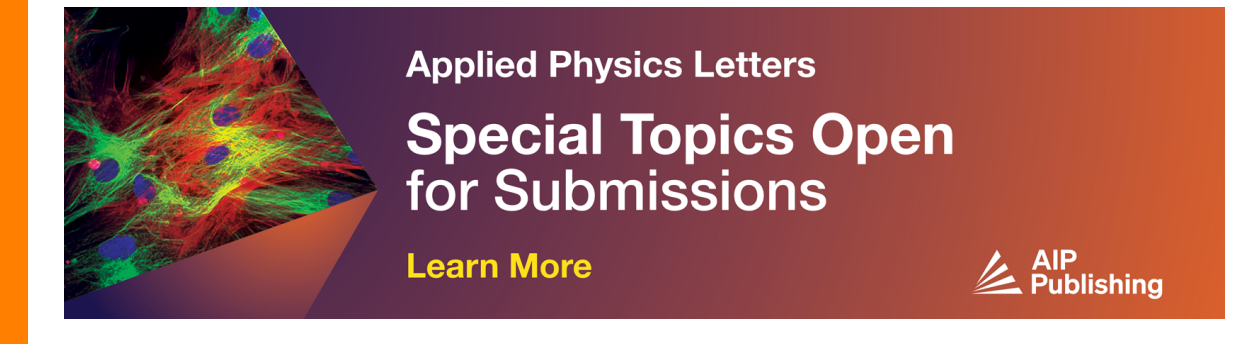
Articles You May Be Interested In

Influence of carrier localization on photoluminescence emission from sub-monolayer quantum dot layers Appl. Phys. Lett. (September 2024)

Influence of non-stoichiometry and local atomic environments on carrier transport in $GaAs_{1-x-y}N_xBi_y$ alloys

Appl. Phys. Lett. (April 2024)

Probing the arsenic distribution and dopant activation in poly-crystalline CdTe_{1-x}Se_x solar cell absorbers *J. Appl. Phys.* (July 2025)





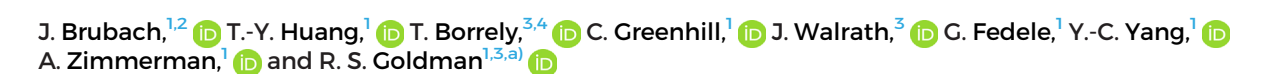
Dopant vs free carrier concentrations in InAs/GaAs semiconductor quantum dots

Cite as: Appl. Phys. Lett. **126**, 112107 (2025); doi: 10.1063/5.0244331 Submitted: 17 October 2024 · Accepted: 6 March 2025 · Published Online: 18 March 2025









AFFILIATIONS

- ¹Department of Materials Science & Engineering, University of Michigan, Ann Arbor, Michigan 48109, USA
- ²Department of Electrical and Computer Engineering, Princeton University, Princeton, New Jersey 08544, USA
- ³Department of Physics, University of Michigan, Ann Arbor, Michigan 48109, USA

ABSTRACT

Semiconductor quantum dots (QDs) are nanostructures that can enhance the performance of electronic devices due to their 3D quantization. Typically, heterovalent impurities, or dopants, are added to semiconducting QDs to provide extra electrons and improve conductivity. Since each QD is expected to contain a few dopants, the extra electrons and their parent dopants have been difficult to locate. In this work, we investigate the spatial distribution of the extra electrons and their parent donors in epitaxial InAs/GaAs QDs using local-electrode atom-probe tomography and self-consistent Schrödinger–Poisson simulations in the effective mass approximation. Although dopants are provided in both layers, the ionized donors primarily reside outside of the QDs, providing extra electrons that are contained within the QDs. Indeed, due to the quantum confinement-induced enhancement of the donor ionization energy within the QDs, a lower fraction of dopants within the QDs are ionized. These findings suggest a pathway toward the development of 3D modulation-doped nanostructures.

Published under an exclusive license by AIP Publishing. https://doi.org/10.1063/5.0244331

Semiconductor quantum dots (QDs)^{1,2} have been shown to enhance the performance of optoelectronic devices, including solar cells, ^{3–8} lasers, ^{9–12} and photodetectors. ^{13–19} Heterovalent doping of QDs has been used to improve carrier collection efficiencies ²⁰ and open-circuit voltages ²¹ of solar cells and to enhance photoresponse, sensitivity, and infrared absorption of photodetectors. ^{22,23} However, for optimum device performance, the precise control of the positions of the parent dopant atoms and the free carriers they provide is needed. ^{21,22} In some cases, fully carrier-depleted QDs have been reported and attributed to nanocrystal "self-purification" mechanisms. ^{24–26} Similarly, carrier depletion has been reported in semiconductor nanowires, especially those with diameters less than the Bohr radius. ^{27–30} Recently, local-electrode atom-probe (LEAP) tomography of silicon nanocrystals (NCs) has revealed dopant distributions that are independent of NC size. ^{31,32}

For epitaxial semiconductor QDs, it has been suggested that dopant incorporation at QD surfaces is energetically favored over incorporation into the QD core. ³³ Furthermore, for Stranski–Krastanow (SK) QD layers, which consist of arrays of 3D islands on top of a 2D alloy layer, a locally reduced carrier concentration has been observed at the 3D islands in comparison with that of the surrounding 2D alloy layers.³⁴ For capped SK-QD layers, depth-dependent carrier concentrations have been attributed to carrier trapping at strain-relaxation induced interfacial dislocations.^{35,36} Meanwhile, it has been suggested that the dopant activation energy is significantly enhanced near the GaAs surface.³⁷ To date, the relative roles of dopant incorporation, dopant activation, and free carrier trapping are not well understood.

Therefore, we consider the relationship between dopant distributions and their activation in the vicinity of QD layers, with and without a GaAs capping layer. Using the local indium and gallium compositions, as well as the silicon atomic concentrations from local-electrode atom-probe (LEAP) tomography as input into self-consistent Schrödinger–Poisson simulations based on the effective mass approximation, we compute the 3D confinement energies and the distributions of ionized dopants and free carriers. Although the parent dopants are observed both within and outside of the QDs, the ionized donors are primarily located outside of the QDs, providing extra electrons that are contained within the QDs. These doped QD nanocomposites provide a pathway toward the development of 3D modulation-doped nanostructures for a variety of applications.

⁴Institute of Physics, University of São Paulo, Rua do Matão 1371, 05508-090 São Paulo, São Paulo, Brazil

a) Author to whom correspondence should be addressed: rsgold@umich.edu

For these investigations, five periods of silicon-doped InAs/GaAs QD superlattices, consisting of alternating layers of InAs (three MLs) and 30 nm GaAs spacers, were deposited on Si-doped GaAs (001) substrates by molecular-beam epitaxy (MBE) using solid Ga, In, and As₂ sources. The parameters for the MBE growth are presented in the supplementary material. Following growth, multiple conical-shaped LEAP specimens ("tips") were prepared using a lift-out process^{38,39} and loaded into a Cameca LEAP 4000XR, which was maintained at cryogenic temperatures (<25 K) under ultra-high vacuum conditions $(3.0 \times 10^{-11} \, \text{Torr})$. LEAP experiments were performed in laser mode with a detection rate of 0.005 ion/pulse, wavelength of 355 nm, pulse rate of 200 kHz, and pulse energy of 1 pJ. To maintain near III-V stoichiometry, a laser pulse energy of 1 pJ, with an estimated $F_{\text{eff}} \approx 21.8 \text{ V/}$ nm, was utilized, consistent with earlier studies. 40-42 The total regionof-interest (ROI) volumes exceeded 30 000 nm3. Three-dimensional reconstructions of the datasets were produced and examined using Cameca's Integrated Visualization and Analysis (IVAS) software AP Suite 6.3. Finally, using the nanostructure volumes and local x_{In} and f_{Si} from LEAP, probability densities, confined state energies, and carrier concentrations were computed using 3D Schrödinger-Poisson simulations in the effective mass approximation at 300 K using nextnano.

To visualize the InGaAs QDs and Si clusters within the QD layers, we present x-z views of LEAP reconstructions [Fig. 1(a)]. The corresponding spatial-averaged 1D profile of x_{Im} reveals maximum x_{In} values of 0.16 for each layer, with $x_{In} \le 0.001$ within the GaAs spacer regions. Meanwhile, in Fig. 1(b), a 2D contour plot, with local x_{In} values averaged over a 2-nm-thick region-of-interest (ROI) vertically centered about the QD layer, reveals \approx 20 nm-sized In_xGa_{1-x}As QDs atop 2D alloy layers, along with ≤ 4 nm-sized silicon clusters. For example, for the SK-QD in Fig. 1(b), the local x_{In} ranges from ≈ 0.24 at the QD edges to ≈ 0.54 at the QD core. Meanwhile, clusters of Si, with diameters of 1-4 nm and Si atomic fraction $(f_{Si}) \approx 0.0075$, are apparent within the QD, 2D alloy layers, and spacer layers. As shown by the arrows in Fig. 1(b), some regions of the SK-QD/matrix interface are diffuse, suggesting the presence of chromatic aberrations in the LEAP reconstruction. 43 Further analysis, including LEAP-informed computations that match physical properties, suggest a minimal impact of the chromatic aberrations on the QD size and shape.

The process for developing nanostructural models for input into the Schrödinger-Poisson simulations³⁹ is illustrated by the x-z and

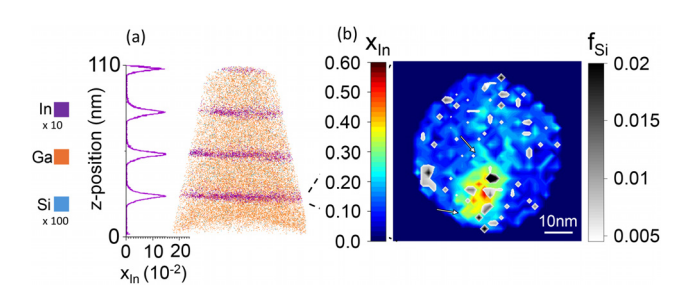


FIG. 1. Local-electrode atom probe (LEAP) data for silicon-doped InGaAs/GaAs multilayers consisting of arrays of Stranski–Krastanow quantum dots, along with clusters of silicon dopants: (a) x–z view of LEAP reconstruction, with In, Ga, and Si atoms are shown as purple, orange, and blue, respectively, and corresponding spatially averaged 1D profile of the In composition, x_{In} . The signals for In and Si are enhanced by 10 and $100\times$ in the 3D x–z view of LEAP reconstruction in (a). (b) 2D contour plot of the In composition, x_{In} , and Si atomic composition, f_{Si} .

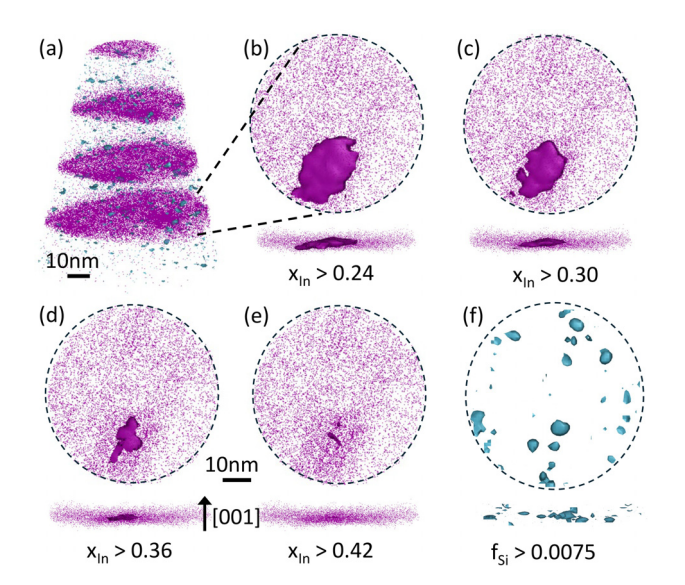


FIG. 2. LEAP isosurfaces for $\ln_x Ga_{1-x} As/GaAs$ SK-QD layers: (a) the entire conical specimen with $x_{ln}>0.24$ (purple) and $f_{Si}>0.0075$ (blue); for an example SK-QD layer, corresponding x–z views are shown for (b) $x_{ln}>0.24$, (c) $x_{ln}>0.30$, (d) $x_{ln}>0.36$, (e) $x_{ln}>0.42$, and (f) $f_{Si}>0.0075$.

x–y isosurfaces, which show regions with composition above the threshold value in Figs. 2(a)–2(f). In Fig. 2(a), the x–z isosurface reveals four SK-QD layers with wetting layers of fixed composition and thickness, as well as clusters of Si distributed both within and between the QD layers. For the first SK-QD layer in Fig. 2(a), x–y and x–z isosurfaces with $x_{In}>0.24$, 0.30, 0.36, and 0.42 are shown in Figs. 2(b)–2(e). The corresponding x–y and x–z isosurfaces with $f_{Si}>0.0075$ are shown in Fig. 2(f). Together, these isosurfaces reveal ≈ 20 nm In $_xGa_{1-x}$ As QDs (x > 0.24) with higher composition "cores" (up to x ≈ 0.54); meanwhile, 1–4 nm diameter silicon clusters are apparent throughout the layer.

As shown in Fig. 3(a), the QD is modeled a series of non-concentric semi-ellipsoids with the x_{In} gradient increasing toward the

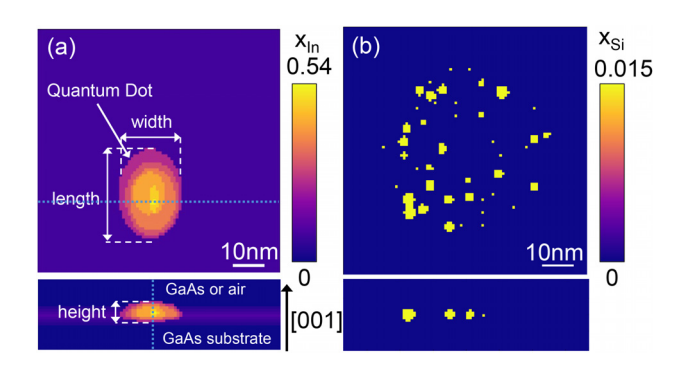


FIG. 3. 2D contour plot of x_{in} and Si clusters used as the models for nextnano simulations. The blue dotted lines in the x-y view images (top) indicate the positions of the x-z view images (bottom). In the simulation, we assume that the Si atoms substitute for Ga atoms, yielding n-type doping. In addition, these blue dotted lines indicate the positions of the CBEs and VBEs plotted along the x- and z-directions in Fig. 4.

QD core, in increments of $x_{In} = 0.06$, from $x_{In} = 0.24$ to $x_{In} = 0.54$, consistent with the iso-surfaces in Fig. 2. In the simulation, substitutional incorporation of Si at group III sites is assumed in the nextnano simulations. The Si clusters are modeled as 1–4 nm diameter spheres with constant x_{Si} of 0.015 substituting the group III sites, shown in Fig. 3(b). For the GaAs layers, 2D contour plots if Si clusters are shown in the supplementary material. The QDs and Si clusters are input as ellipsoids and spheres, respectively. For the capped QDs, the layer on top of the QD is GaAs; for the uncapped QDs, the layer is "air." The nextnano approximation to a grid spacing of 0.8 nm leads to the apparent pixelated appearance of Fig. 3. The lattice parameters, effective masses, band edges, and deformation potentials used in the nextnano simulations are available in the supplementary material.

For the capped and uncapped QD layers, the conduction-band edge (CBE, red), valence band edge (VBE, blue), and ground states for electrons and holes, computed along the blue dotted lines intersecting the QD in Fig. 3(a), are shown in Figs. 4(a) and 4(c) and 4(b) and 4(d), respectively. For each of the x-, y-, and z-directions, if the electron (hole) level is below (above) the edge of the conduction (valence) band, the carrier is considered to be confined. For the capped QD layers, the computed CBE and VBE reveal that E_{e1} (E_{hh1}) lies 47 meV (90 meV) below (above) the CBE (VBE) of the surrounding 2D alloy layers ($x_{In} = 0.08$) in the x-direction, and 114 meV (167 meV) below (above) the CBE (VBE) of the 2D alloy layers in the z-direction.

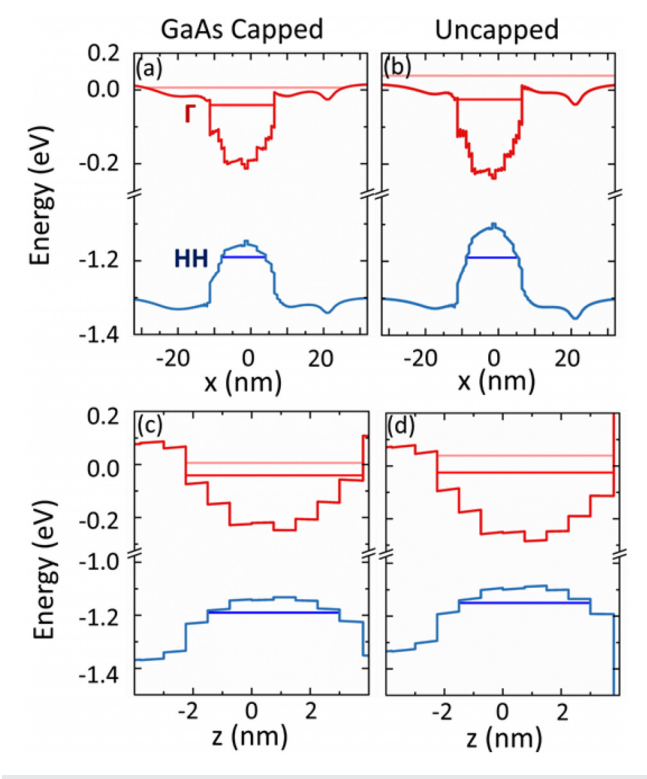


FIG. 4. Computed spatial-dependence of the conduction-band edge (CBE, red), valence band edge (VBE, blue), and corresponding confined electron ground and first excited (E_{e1} and E_{e2}) and confined hole ground (E_{hh1}) states for the (a) and (c) capped and (b) and (d) uncapped QD layers. Plots (a) and (b) [(c) and (d)] illustrate the x-dependence (z-dependence) of the band edges computed along the blue dotted lines intersecting the QD in Fig. 3(a).

Therefore, for the capped QD layers, 3D confinement of electrons and holes is confirmed. The first electron excited state (Ee2) lies 12 meV above CBE of the 2D alloy layers in the x-direction and 60 meV below CBE of the 2D alloy layers in the z-direction. Since the $E_{\rm e2}$ is above the CBE in x-direction, only the ground state is confined in the QD. For the uncapped QD layers, the computed CBE and VBE reveal that $\rm E_{e1}$ (E_{hh1}) lies 52 meV (123 meV) below (above) the CBE (VBE) of the surrounding 2D alloy layers ($x_{In} = 0.08$) in the x-direction, and 86 meV (148 meV) below (above) the CBE (VBE) of the 2D alloy layers in the z-direction. Thus, 3D confinement of electrons and holes for the uncapped QD layer is also confirmed. The first electron excited state (Ee2) lies 27 meV above CBE of the 2D alloy layers in the x-direction and 16 meV below CBE of the 2D alloy layers in the z-direction. Since the Ee2 is above the CBE in x-direction, only the ground state is confined in the QD. For the uncapped QD layer, the higher energy barrier (>7 eV) at z = 3.3 nm is due to the "air" at the free surface.

We now consider the spatial distribution of ionized donors and free carriers in the capped and uncapped QD layers (Fig. 5). For the capped QD layers, Fig. 5(a) reveals clusters of ionized donors in the x-y (top) and x-z (bottom) views, with the lowest fraction of ionized donors located inside the white dashed ellipses that correspond to the positions of the QDs. Similarly, for the uncapped QD layers, Fig. 5(b) reveals clusters of ionized donors in the x-y (top) and x-z (bottom) views, with the lowest fraction of ionized donors located inside the QDs. For the GaAs layers, dopant ionization is shown in the supplementary material. The lower fraction of dopant ionization inside the QDs is due to quantum confinement that enhances the donor ionization energy. ¹⁹ On the contrary, the free carriers are highly concentrated inside the QDs, as shown in Figs. 5(c) and 5(d). Since the free carriers are concentrated inside the

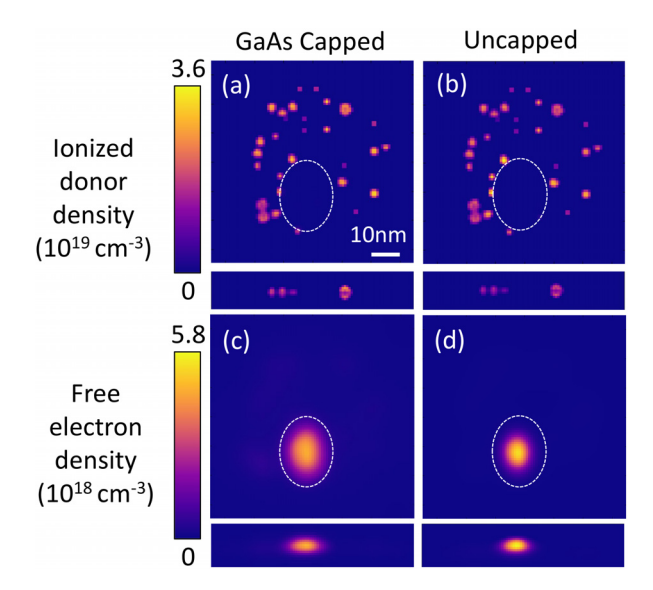


FIG. 5. Computed densities of ionized donors and free electrons for (a) and (c) capped and (b) and (d) uncapped QD layers. The white dashed ellipse indicates the position of the QDs, and the maximum value of the color scales for the ionized donor and free electron densities are shown in the upper right corner. For the ionized donors in (a) and (b), the highest densities are outside the QDs. Meanwhile, for the free electrons in (c) and (d), the highest densities are within the QDs. The lower fraction of dopant ionization inside the QDs is due to quantum confinement that enhances the donor ionization energy.

QDs, but the ionized donors are primarily located outside the QDs, these QD layers act as modulation-doped nanostructures with dopants from the 2D alloy layers providing free carriers.

Finally, we compare the free carrier densities for the capped [Fig. 5(c)] and uncapped [Fig. 5(d)] QD layers. The higher free carrier density for the uncapped QD layers is presumably due to the higher energy barrier (>7 eV) at $z=3.3\,\mathrm{nm}$ [Fig. 4(d)], which does not allow the tunneling of the electrons. To determine the number of electrons inside the QD, we integrated the ground state electron density inside the QD, yielding 2.7 and 1.7 electrons inside the capped and uncapped SK-QDs, respectively. The capped QDs have more electrons because the n-type GaAs:Si capping layer provides additional electrons. In contrast, lateral gradients in carrier concentration were reported for uncapped QDs, ³⁴ with full carrier depletion reported for sufficiently large capped QDs. ³⁶ Therefore, future simulations need to include contributions from surface and/or interface electronic states.

In summary, we have examined the relationship between dopant distributions and their activation in the vicinity of InAs/GaAs QD layers. We used local x_{In} compositions and f_{Si} compositions from LEAP tomography as input into self-consistent Schrödinger–Poisson simulations based on the effective mass approximation to compute 3D confinement energies and distributions of ionized dopants and free carriers. Although Si dopants are located within the QDs and surrounding 2D alloy layers, dopant ionization is lowest inside the QDs. Interestingly, the free electron concentration is highest within the QD but is reduced in the presence of a GaAs capping layer due to the tunneling of electrons from the QD to the GaAs capping layer. This study provides insight into the relative roles of dopant incorporation, dopant activation, and free carrier trapping in the vicinity of nanostructures, offering a pathway toward the development of 3D modulation-doped nanocomposites.

See the supplementary material for details on molecular-beam epitaxy, selection of LEAP parameters, LEAP chromatic aberrations, 1D composition profiles across QDs and Si clusters, nextnano input parameters, and computed ionized donors in GaAs spacer layers.

J. Brubach's work at the University of Michigan was supported by Intel's University Research & Collaboration Office and by Maria Goeppert Mayer Collegiate Professorship funds. T.-Y. Huang, T. Borrely, and R. S. Goldman were supported in part by the Air Force Office of Scientific Research through the Multidisciplinary University Research Initiative, Award No. FA9550-23-1-0334. T.-Y. Huang and Y.-C. Yang were also supported in part by the Chia-Lun Lo Fellowship from the Rackham Graduate School at the University of Michigan. C. Greenhill and J. Walrath were supported by National Science Foundation (NSF) Graduate Student Research Fellowships under Grant No. DGE 1256260. G. Fedele was supported by an REU supplement to NSF Grant No. ECCS-1610362. The authors acknowledge the assistance of Professor Baishakhi Mazumder at the University at Buffalo and staff at the Michigan Center for Materials Characterization at the University of Michigan.

AUTHOR DECLARATIONS Conflict of Interest

The authors have no conflicts to disclose.

Author Contributions

J. Brubach and T.-Y. Huang contributed equally to this work.

J. Brubach: Data curation (lead); Formal analysis (lead); Investigation (lead); Methodology (lead); Software (lead); Visualization (lead); Writing – original draft (lead); Writing – review & editing (equal). T.-Y. Huang: Conceptualization (lead); Data curation (equal); Formal analysis (equal); Investigation (equal); Methodology (equal); Software (equal); Visualization (equal); Writing – original draft (equal); Writing – review & editing (equal). T. Borrely: Data curation (equal); Formal analysis (equal); Methodology (equal). C. Greenhill: Data curation (equal); Formal analysis (equal); Software (equal). J. Walrath: Conceptualization (equal); Data curation (equal); Formal analysis (equal); Methodology (equal). G. Fedele: Data curation (equal); Formal analysis (equal); Software (equal). Y.-C. Yang: Formal analysis (equal); Software (equal). A. Zimmerman: Software (equal). R. S. Goldman: Funding acquisition (lead); Project administration (lead); Resources (lead); Supervision (lead); Writing – review & editing (lead).

DATA AVAILABILITY

The data that support the findings of this study are available within the article and its supplementary material.

REFERENCES

- ¹I. Ramiro, J. Villa, P. Lam, S. Hatch, J. Wu, E. Lopez, E. Antolin, H. Liu, A. Marti, and A. Luque, "Wide-bandgap InAs/InGaP quantum-dot intermediate band solar cells," IEEE J. Photovoltaics 5, 840 (2015).
- ²M. J. da Silva, A. A. Quivy, S. Martini, T. E. Lamas, E. C. F. da Silva, and J. R. Leite, "Optical response at 1.3m and 1.5m with InAs quantum dots embedded in a pure GaAs matrix," J. Cryst. Growth 251, 181 (2003).
- ³Y. Shoji, R. Tamaki, and Y. Okada, "Multi-stacked GaSb/GaAs type-II quantum nanostructures for application to intermediate band solar cells," AIP Adv. 7, 065305 (2017).
- ⁴G. Yang, W. Liu, Y. Bao, X. Chen, C. Ji, B. Wei, F. Yang, and X. Wang, "Performance optimization of In(Ga)As quantum dot intermediate band solar cells," Discover Nano 18, 67 (2023).
- ⁵N. Alnami, R. Kumar, A. Kuchuk, Y. Maidaniuk, S. K. Saha, A. A. Alnami, R. Alhelais, A. Kawagy, M. E. Ware, Y. I. Mazur, and G. J. Salamo, "InAs nanostructures for solar cell: Improved efficiency by submonolayer quantum dot," Sol. Energy Mater. Sol. Cells 224, 111026 (2021).
- ⁶T. Aho, F. Elsehrawy, A. Tukiainen, S. Ranta, M. Raappana, R. Isoaho, A. Aho, A. Hietalahti, F. Cappelluti, and M. Guina, "Thin-film InAs/GaAs quantum dot solar cell with planar and pyramidal back reflectors," Appl. Opt. 59, 6304 (2020).
- 7S. R. Tatavarti, Z. S. Bittner, A. Wibowo, M. A. Slocum, G. Nelson, H. Kum, S. P. Ahrenkiel, and S. M. Hubbard, "Epitaxial lift-off (ELO) of InGaP/GaAs/InGaAs solar cells with quantum dots in GaAs middle sub-cell," Sol. Energy Mater. Sol. Cells 185, 153 (2018).
- ⁸T. Borrely, A. Alzeidan, M. De Lima, G. Jacobsen, T.-Y. Huang, Y.-C. Yang, T. Cantalice, R. Goldman, M. Teodoro, and A. Quivy, "Viability of intermediate band solar cells based on InAs/GaAs submonolayer quantum dots and the role of surface reconstruction," Sol. Energy Mater. Sol. Cells 254, 112281 (2023).
- ⁹Z. Mi, P. Bhattacharya, and S. Fathpour, "High-speed 1.3m tunnel injection quantum-dot lasers," Appl. Phys. Lett. **86**, 153109 (2005).
- 10 J. C. Norman, R. P. Mirin, and J. E. Bowers, "Quantum dot lasers—History and future prospects," J. Vac. Sci. Technol. A 39, 020802 (2021).
- ¹¹J. Yang, Z. Liu, P. Jurczak, M. Tang, K. Li, S. Pan, A. Sanchez, R. Beanland, J.-C. Zhang, H. Wang, F. Liu, Z. Li, S. Shutts, P. Smowton, S. Chen, A. Seeds, and H. Liu, "All-MBE grown InAs/GaAs quantum dot lasers with thin Ge buffer layer on Si substrates," J. Phys. D 54, 035103 (2021).
- ¹²H. Deng, L. Jarvis, Z. Li, Z. Liu, M. Tang, K. Li, J. Yang, B. Maglio, S. Shutts, J. Yu, L. Wang, S. Chen, C. Jin, A. Seeds, H. Liu, and P. M. Smowton, "The role of

- different types of dopants in 1.3 m InAs/GaAs quantum-dot lasers," J. Phys. D 55, 215105 (2022).
- ¹³J. Phillips, K. Kamath, and P. Bhattacharya, "Far-infrared photoconductivity in self-organized InAs quantum dots," Appl. Phys. Lett. 72, 2020 (1998).
- ¹⁴J. Liu, F. Wang, S. Zhai, J. Zhang, S. Liu, J. Liu, L. Wang, F. Liu, and Z. Wang, "Normal-incidence quantum cascade detector coupled by nanopore structure," Appl. Phys. Express 11, 042001 (2018).
- ¹⁵B. F. Levine, "Quantum-well infrared photodetectors," J. Appl. Phys. 74, R1 (1993).
- ¹⁶M. P. Touse, G. Karunasiri, K. R. Lantz, H. Li, and T. Mei, "Near- and mid-infrared detection using GaAs/In_xGa_{1-x}As/InyGa_{1-y}As multiple step quantum wells," Appl. Phys. Lett. 86, 093501 (2005).
- ¹⁷A. Alzeidan, T. Cantalice, K. Sautter, K. Vallejo, P. Simmonds, and A. Quivy, "High-performance infrared photodetector based on InAs/GaAs submonolayer quantum dots grown at high temperature with a (2 × 4) surface reconstruction," Sens. Actuators A 374, 115464 (2024).
- ¹⁸T. Murata, S. Asahi, S. Sanguinetti, and T. Kita, "Infrared photodetector sensitized by InAs quantum dots embedded near an Al_{0.3}Ga_{0.7}As/GaAs heterointerface," Sci. Rep. 10, 11628 (2020).
- ¹⁹S.-Y. Lin, Y.-J. Tsai, and S.-C. Lee, "Effect of silicon dopant on the performance of InAs/GaAs quantum-dot infrared photodetectors," Jpn. J. Appl. Phys. 43, L167 (2004).
- ²⁰T. Li, H. Lu, L. Fu, H. H. Tan, C. Jagadish, and M. Dagenais, "Enhanced carrier collection efficiency and reduced quantum state absorption by electron doping in self-assembled quantum dot solar cells," Appl. Phys. Lett. 106, 053902 (2015).
- ²¹S. Naito, K. Yoshida, N. Miyashita, R. Tamaki, T. Hoshii, and Y. Okada, "Effect of Si doping and sunlight concentration on the performance of InAs/GaAs quantum dot solar cells," J. Photonics Energy 7, 025505 (2017).
- quantum dot solar cells," J. Photonics Energy 7, 025505 (2017).

 22 X. Zhang, V. Mitin, A. Sergeev, K. Sablon, A. Varghese, M. Yakimov, V. Tokranov, and S. Oktyabrsky, "Effects of doping on photoelectron kinetics and characteristics of quantum dot infrared photodetector," Proc. SPIE 10177, 1017729 (2017).
- ²³K. Sablon, A. Sergeev, N. Vagidov, A. Antipov, J. Little, and V. Mitin, "Effective harvesting, detection, and conversion of IR radiation due to quantum dots with built-in charge," Nanoscale Res. Lett. 6, 584 (2011).
- ²⁴S. C. Erwin, L. Zu, M. I. Haftel, A. L. Efros, T. A. Kennedy, and D. J. Norris, "Doping semiconductor nanocrystals," Nature 436, 91 (2005).
- ²⁵G. M. Dalpian and J. R. Chelikowsky, "Self-purification in semiconductor nanocrystals," Phys. Rev. Lett. 96, 226802 (2006).
- ²⁶J. P. Petropoulos, T. R. Cristiani, P. B. Dongmo, and J. M. O. Zide, "A simple thermodynamic model for the doping and alloying of nanoparticles," Nanotechnology 22, 245704 (2011).
- ²⁷G. W. Bryant, "Hydrogenic impurity states in quantum-well wires," Phys. Rev. B 29, 6632 (1984).
- ²⁸R. Loudon, "One-dimensional hydrogen atom," Am. J. Phys. 27, 649 (1959).
- ²⁹A. Echresh, H. Arora, F. Fuchs, Z. Li, R. Hübner, S. Prucnal, J. Schuster, P. Zahn, M. Helm, S. Zhou, A. Erbe, L. Rebohle, and Y. M. Georgiev, "Electrical

- characterization of germanium nanowires using a symmetric hall bar configuration: Size and shape dependence," Nanomaterials 11, 2917 (2021).
- ³⁰S. Alagha, S. Heedt, D. Vakulov, F. Mohammadbeigi, E. S. Kumar, T. Schäpers, D. Isheim, S. P. Watkins, and K. L. Kavanagh, "Electrical properties of lightly Ga-doped ZnO nanowires," Semicond. Sci. Technol. 32, 125010 (2017).
- ³¹R. Demoulin, M. Roussel, S. Duguay, D. Muller, D. Mathiot, P. Pareige, and E. Talbot, "Atomic-scale characterization of N-doped Si nanocrystals embedded in SiO² by atom probe tomography," J. Phys. Chem. C 123, 7381 (2019).
- ³²H. Gnaser, "Atom probe tomography of nanostructures," Surf. Interface Anal. 46, 383 (2014).
- ³³V. D. Dasika, A. V. Semichaevsky, J. P. Petropoulos, J. C. Dibbern, A. M. Dangelewicz, M. Holub, P. K. Bhattacharya, J. M. O. Zide, H. T. Johnson, and R. S. Goldman, "Influence of Mn dopants on InAs/GaAs quantum dot electronic states," Appl. Phys. Lett. 98, 141907 (2011).
- ³⁴J. C. Walrath, Y.-H. Lin, S. Huang, and R. S. Goldman, "Profiling the local carrier concentration across a semiconductor quantum dot," Appl. Phys. Lett. 106, 192101 (2015).
- 35Y. Chen, X. W. Lin, Z. Liliental-Weber, J. Washburn, J. F. Klem, and J. Y. Tsao, "Dislocation formation mechanism in strained In_xGa_{1-x}As islands grown on GaAs(001) substrates," Appl. Phys. Lett. 68, 111 (1996).
- 36J. S. Wang, J. F. Chen, J. L. Huang, P. Y. Wang, and X. J. Guo, "Carrier distribution and relaxation-induced defects of InAs/GaAs quantum dots," Appl. Phys. Lett. 77, 3027 (2000).
- 37A. P. Wijnheijmer, J. K. Garleff, K. Teichmann, M. Wenderoth, S. Loth, R. G. Ulbrich, P. A. Maksym, M. Roy, and P. M. Koenraad, "Enhanced donor binding energy close to a semiconductor surface," Phys. Rev. Lett. 102, 166101 (2009).
- 38T. Borrely, T.-Y. Huang, Y.-C. Yang, R. S. Goldman, and A. A. Quivy, "On the importance of atom probe tomography for the development of new nanoscale devices," in 36th Symposium on Microelectronics Technology (SBMICRO) (IEEE, Porto Alegre, Brazil, 2022), p. 1.
- ³⁹T.-Y. Huang, T. Borrely, Y.-C. Yang, A. Alzeidan, G. M. Jacobsen, M. D. Teodoro, A. A. Quivy, and R. S. Goldman, "Influence of carrier localization on photoluminescence emission from sub-monolayer quantum dot layers," Appl. Phys. Lett. 125, 122108 (2024).
- ⁴⁰J. W. Mitchell, C. M. Greenhill, T.-Y. Huang, T. Jen, Y.-C. Yang, K. Hammond, J. N. Heyman, and R. S. Goldman, "Influence of non-stoichiometry and local atomic environments on carrier transport in GaAs_{1-x-y}N_xBi_y alloys," Appl. Phys. Lett. **124**, 152108 (2024).
- ⁴¹D. R. Kingham, "The post-ionization of field evaporated ions: A theoretical explanation of multiple charge states," Surf. Sci. 116, 273 (1982).
- ⁴²E. Di Russo, I. Blum, J. Houard, G. Da Costa, D. Blavette, and L. Rigutti, "Field-dependent measurement of GaAs composition by atom probe tomography," Microsc. Microanal. 23, 1067 (2017).
- ⁴³E. A. Marquis and F. Vurpillot, "Chromatic aberrations in the field evaporation behavior of small precipitates," Microsc. Microanal. 14, 561 (2008).